

# Analytical study of dynamics of matter-wave solitons in lossless nonlinear discrete bi-inductance transmission lines

E. Kengne and A. Lakhssassi

*Département d'Informatique et d'Ingénierie, Université du Québec en Outaouais, 101 St-Jean-Bosco, Succursale Hull, Gatineau, Quebec, Canada J8Y 3G5*

(Received 11 December 2014; published 12 March 2015)

We consider a lossless one-dimensional nonlinear discrete bi-inductance electrical transmission line made of  $N$  identical unit cells. When lattice effects are considered, we use the reductive perturbation method in the semidiscrete limit to show that the dynamics of modulated waves can be modeled by the classical nonlinear Schrödinger (CNLS) equation, which describes the modulational instability and the propagation of bright and dark solitons on a continuous-wave background. Our theoretical analysis based on the CNLS equation predicts either two or four frequency regions with different behavior concerning the modulational instability of a plane wave. With the help of the analytical solutions of the CNLS equation, we investigate analytically the effects of the linear capacitance  $C_S$  on the dynamics of matter-wave solitons in the network. Our results reveal that the linear parameter  $C_S$  can be used to manipulate the motion of bright, dark, and kink soliton in the network.

DOI: [10.1103/PhysRevE.91.032907](https://doi.org/10.1103/PhysRevE.91.032907)

PACS number(s): 05.45.Yv, 42.65.Tg, 42.25.Bs, 84.40.Az

## I. INTRODUCTION

Because of its wide significance in a great variety of physical systems, the propagation of nonlinear matter waves in nonlinear dispersive media has been the subject of considerable interest for many decades [1–11]. On the other hand, nonlinear discrete electrical transmission lines (NLDETLs) are very convenient tools to study soliton propagation in one-dimensional nonlinear dispersive media [3,5,12–17]. Indeed, NLDETLs are systems where solitons are easily and directly observed in controlled laboratory experiments. They provide a useful way to check how the nonlinear excitations behave inside the nonlinear medium and to model the exotic properties of new systems [5]. This paper contributes to the understanding of this mechanism.

A nonlinear discrete transmission line is comprised of a transmission line periodically loaded with varactors, where the capacitance nonlinearity arises from the variable depletion layer width, which depends both on the dc bias voltage and on the ac voltage of the propagating wave. For example, the model shown in Fig. 1 is a one-dimensional (1D) lossless discrete nonlinear transmission line made of ladder-type  $LC$  circuits containing constant inductors and voltage-dependent capacitors [15,17,18]. The nonlinear capacitors are usually reverse-biased capacitance diodes.

The NLDETL of Fig. 1, which differs from the Hirota-Suzuki model [19] by the presence of a linear dispersive capacitance  $C_S$ , was built by Noguchi to study experimentally the propagation of the first-order Korteweg–de Vries (KdV) solitons [20]. Ichikawa *et al.* [21] used this network to carry out theoretical studies on the motion of the second-order KdV solitons. Employing the Noguchi model of Fig. 1, Yoshinaga and Kakutani [22] generalized the Toda potential to study experimentally the properties of the second-order KdV solitons. Exploiting the Patheria-Morris method, Pelap and Faye [18] showed that the discrete network of Fig. 1 can support solitary waves. Using the Kengne-Liu model [17] of wave propagation on the Noguchi model, Marklund and Shukla [23] investigated the modulational instability of partially coherent signals in electrical transmission lines of Fig. 1. It appears that in all

these studies on the network of Fig. 1, the effects of the linear dispersive capacitance  $C_S$  on soliton propagation have not been pointed out.

The main purpose of this paper is to study analytically the effects of the linear dispersive capacitance  $C_S$  on solitary waves propagating on the network of Fig. 1. The paper is organized as follows. In Sec. II we use the reductive perturbation method in the semidiscrete limit to derive a classical nonlinear Schrödinger equation describing the propagation of modulated waves in the network. Then we obtain the general expressions of the bright and dark solitary-wave solutions on a continuous-wave background for the derived CNLS equation and discuss the dynamics of bright and dark one-dimensional solitary waves in Sec. III. The paper is summarized in Sec. IV.

## II. BASIC EQUATIONS AND THE NONLINEAR SCHRÖDINGER MODEL

We consider the 1D lossless discrete nonlinear electrical network of Fig. 1, made of  $N$  identical cells. In this network, the nonlinear capacitance  $C(V_n) = dQ_n/dt$ , where  $Q_n = Q_n(V_n)$  is the corresponding nonlinear charge. In the weakly nonlinear case, we assume that  $Q_n(V_n) = C_0(V_n - \alpha V_n^2 + \beta V_n^3)$ , where  $C_0$  is the characteristic capacitance and the nonlinear coefficients  $\alpha$  and  $\beta$  are positive constants. Applying Kirchhoff's laws on the network of Fig. 1 yields the system of nonlinear discrete equations

$$\frac{d^2 Q_n}{dt^2} + \frac{1}{L_2} V_n - \left[ \frac{1}{L_1} + \frac{C_S}{C_0} \frac{d^2}{dt^2} \right] (V_{n-1} - 2V_n + V_{n+1}) = 0, \quad (1)$$

$n = 1, 2, \dots, N$ . In the linear approximation, the ansatz  $V_n \sim \exp[i(kn - \omega t)]$  leads to the linear dispersion relation of a typical passband filter

$$\omega^2 L_1 L_2 \left( C_0 + 4C_S \sin^2 \frac{k}{2} \right) - \left( L_1 + 4L_2 \sin^2 \frac{k}{2} \right) = 0. \quad (2)$$

In this paper, we restrict ourselves to the network of Fig. 1 for which the dispersion parameter  $C_S$  satisfies the condition  $C_S < \frac{L_2}{L_1} C_0$ , so the group velocity  $v_g = \frac{d\omega}{dk}$  will remain positive

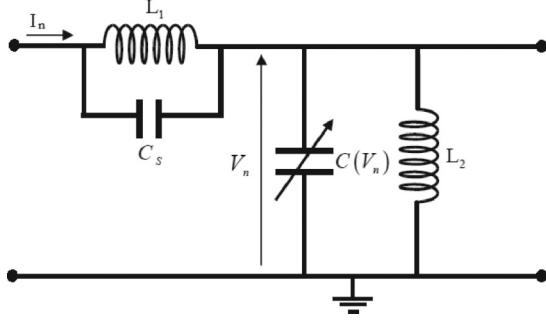


FIG. 1. Schematic representation of one elementary cell of a lossless discrete nonlinear bi-inductance transmission line consisting of four elements: one linear inductor  $L_1$  in parallel with a linear capacitance  $C_s$  in the series branch and one linear inductance  $L_2$  in parallel with a nonlinear capacitor  $C(V)$  in the shunt branch.

throughout our investigation. In the numerical simulations, we will use the typical line parameters [3,24,25]

$$\begin{aligned} L_1 = 28 \mu\text{H}, \quad L_2 = 14 \mu\text{H}, \quad C_0 = 540 \text{ pF}, \quad V_0 = 1.5 \text{ V}, \\ \alpha = 0.16 \text{ V}^{-1}, \quad \beta = 0.0197 \text{ V}^{-2}, \quad C_S \in [0, C_0/2[ \text{ pF}. \end{aligned} \quad (3)$$

With the use of line parameters (3), the linear dispersion curves of a typical passband filter are represented in Fig. 2 for different values of the dispersion coefficient  $C_S$ . These dispersion curves show (a) the frequency  $f = \omega/2\pi$  and (b) the dispersion coefficient  $P_l = d^2\omega/dk^2$  as functions of wave vector  $k$ . The plots of Fig. 2(a) show that the frequency decreases as the dispersion parameter  $C_S$  increases. Plots showing the evolution of the dispersion coefficient  $P_l$  show that for any dispersion parameter  $C_S \in [0, C_0/2[$ , the equation  $P_l(k) = 0$  admits one and only one solution  $k_z \in [0, \pi]$  corresponding to frequency  $f_z = f(k_z)$ ; moreover,  $k_z \rightarrow 1/2$  as  $C_S \rightarrow C_0/2 - 0$ .

Restricting ourselves to waves with a slowly varying envelope in time and space with regard to a given carrier wave with angular frequency  $\omega = 2\pi f$  and wave number  $k$ ,

we introduce the slow envelope variables

$$\xi = \varepsilon(n - v_g t), \quad \tau = \varepsilon^2 t \quad (4)$$

that allow us to apply the reductive perturbation method [6,17]; here  $\varepsilon$  is a small parameter and  $n$  is the cell number. The solution of (1) is then sought in the general form

$$\begin{aligned} V_n(t) = \varepsilon V_{01}(\xi, \tau) \exp(i\theta) + \varepsilon^2 [V_{02}(\xi, \tau) \\ + V_{12}(\xi, \tau) \exp(2i\theta)] + \text{c.c.}, \end{aligned} \quad (5)$$

where  $\theta = kn - \omega t$  is the rapidly varying phase [ $k$  and  $\omega$  are, respectively, the wave vector and the angular frequency satisfying the dispersion relation (2)] and c.c. stands for complex conjugation. The  $\varepsilon^2$  terms are added to the dc term (i.e.,  $\varepsilon$  term) in order to take into account the asymmetry of the charge-voltage relation given by Eq. (1).

Inserting the ansatz (5) into the nonlinear discrete equations (1), neglecting consistently high-order  $\varepsilon$  terms, and keeping up to the second-order derivative terms of  $V_n(t)$  (this is done in order to balance dispersion and nonlinearity) leads to

$$V_{02}(\xi, \tau) = -\frac{\Delta_{02}}{\alpha} |V_{01}|^2, \quad (6a)$$

$$V_{12}(\xi, \tau) = \frac{\alpha\omega^2}{\Delta_{12}} (V_{01})^2, \quad (6b)$$

$$i \frac{\partial V_{01}}{\partial \tau} + P \frac{\partial^2 V_{01}}{\partial \xi^2} + Q |V_{01}|^2 V_{01} = 0, \quad (6c)$$

where

$$\Delta_{02} = \frac{2L_1 C_0 \alpha^2 \omega v_g^2}{1 - L_1 C_0 v_g^2}, \quad (7a)$$

$$\begin{aligned} \Delta_{12} = \omega^2 - \frac{1}{4L_2 C_0} + \frac{(4L_1 C_S \omega^2 - 1) \sin^2 k}{L_1 C_0}, \\ P = -\frac{v_g^2}{2\omega} \left( 1 + \frac{4C_S}{C_0} \sin^2 \frac{k}{2} \right) \\ + \left( \frac{1}{2L_1 C_0 \omega} - \frac{C_S}{2C_0} \omega \right) \cos k - 2 \frac{C_S}{C_0} v_g \sin k, \end{aligned} \quad (7b)$$

$$Q = \frac{3\beta}{2} \omega + \Delta_{02} - \frac{\alpha^2 \omega^3}{\Delta_{12}}. \quad (7c)$$

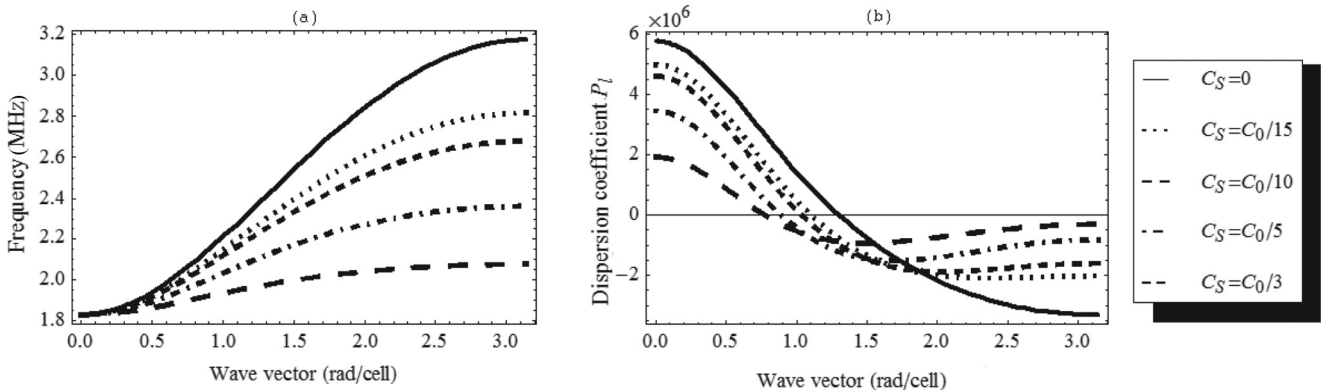


FIG. 2. Theoretical linear dispersion curves showing (a) the frequency  $f = \frac{\omega}{2\pi}$  and (b) the dispersion coefficient  $P_l = \frac{d^2\omega}{dk^2}$  as functions of the wave vector  $k$  for different values of the dispersive parameter  $C_S$ . The line parameters used in these plots are given in Eq. (3).

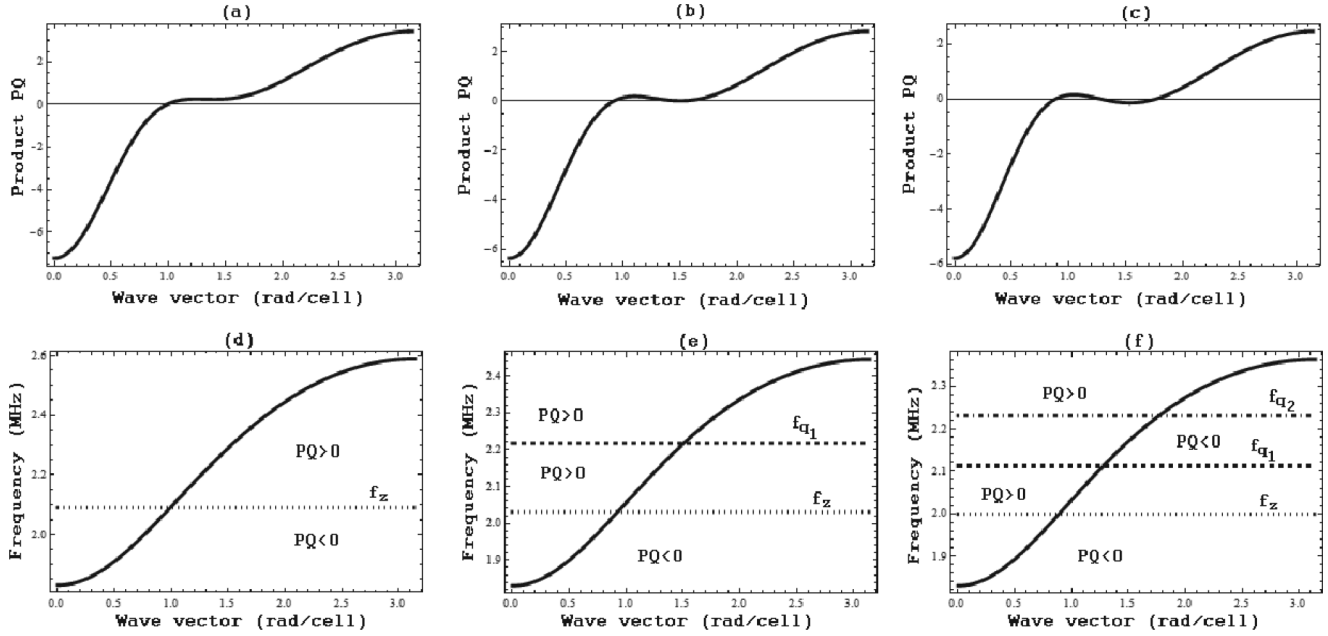


FIG. 3. (a)–(c) Plots of the product  $PQ$  and (d)–(f) theoretical linear dispersion curves as functions of the wave vector  $k$  showing different scenarios of the regions of modulational instability of the soliton wave solutions of the CNLS equation (6c) with the nonlinear coefficient (7c): product  $PQ$  and frequency  $f = \omega/2\pi$  for (a) and (d)  $C_S = C_0/8 < C_S^0$ , (b) and (e)  $C_S = C_S^0 \approx C_0/5.8675457875$ , and (c) and (f)  $f = \omega/2\pi$  for  $C_S = C_0/5 > C_S^0$ . To generate these plots, we have used the line parameters (3).

It follows from Eqs. 6(a), 6(b), 7(a), and 7(c) that the two last terms in the expression of the nonlinear coefficient  $Q$  of the CNLS equation (6c) come from the  $\varepsilon^2$  terms in the general expression (5) for  $V_n(t)$ . As one can see from the expression 7(b), the  $\varepsilon^2$  terms do not affect the dispersion coefficient  $P$ . This means that assuming a solution of the form (5) without  $\varepsilon^2$  terms leads to another CNLS equation similar to (6c), except for the nonlinear coefficient, which is

$$Q = \frac{3\beta}{2}\omega. \quad (8)$$

We have thus obtained two classical nonlinear Schrödinger equations with the same dispersion coefficient, but different nonlinear coefficient allowing us to investigate the dynamics of matter-wave solitons on the network of Fig. 1. Applying the modulational instability criterion for the CNLS equation [26], we conclude that a uniform wave train propagating along the dispersive network of Fig. 1 will become unstable under the modulation for  $PQ > 0$  and will remain stable under the modulation for  $PQ < 0$ . Because the nonlinear coefficient  $Q$  defined by Eq. (8) does not change sign when  $\omega$  maintains its sign, the sign of the product  $PQ$  in Fig. 3(b) coincides with that of  $P$ . For the nonlinear coefficient  $Q$  defined by Eq. (7c), we have three scenarios:  $\max_{[0,\pi]} Q(k) = Q_{\max}(C_S)$  is an increasing continuous function of variable  $C_S$ ; moreover,  $Q_{\max}(0) < 0 < Q_{\max}(C_0/2)$ ; therefore, there exists a unique  $C_S = C_S^0 \in [0, C_0/2]$  such that  $Q_{\max}(C_S^0) = 0$ . For every  $C_S < C_S^0$  we will have  $Q(k) < 0$ , while for every  $C_S > C_S^0$ , the equation  $Q(k) = 0$  will have two solutions  $k_{q_1}$  and  $k_{q_2}$  on  $[0, \pi]$ . Different scenarios of the region of modulational instability of the soliton-wave solution of the CNLS equation (6c) with the nonlinear coefficient (7c) are presented in Fig. 3.

In Fig. 3,  $f_z = f(k_z)$ , where  $P(k_z) = 0$ , while  $f_{q_1}$  and  $f_{q_2}$  are the frequencies associated with  $Q(k) = 0$ . Figure 3(d) shows two regions of modulational instability: the region of  $f \in [f_{\min}, f_z[$  corresponding to  $PQ < 0 \rightarrow$  stable  $\rightarrow$  hole solitons and the region  $f \in ]f_z, f_{\max}]$  corresponding to  $PQ > 0 \rightarrow$  unstable  $\rightarrow$  envelope solitons. In Fig. 3(e) we observe two regions of modulational instability: the region  $f \in [f_{\min}, f_z[$  corresponding to  $PQ < 0 \rightarrow$  stable  $\rightarrow$  hole solitons and the region  $f \in ]f_z, f_{q_1}[ \cup ]f_{q_1}, f_{\max}[$  corresponding to  $PQ > 0 \rightarrow$  unstable  $\rightarrow$  envelope solitons. Figure 3(f) reveals four regions of modulational instability: the regions  $f \in [f_{\min}, f_z[$  and  $f \in ]f_{q_1}, f_{q_2}[$  corresponding to  $PQ < 0 \rightarrow$  stable  $\rightarrow$  hole solitons and regions  $f \in ]f_z, f_{q_1}[$  and  $f \in ]f_{q_2}, f_{\max}]$  corresponding to  $PQ > 0 \rightarrow$  unstable  $\rightarrow$  envelope solitons.

Figure 4 shows the product  $PQ$  as a function of the wave vector  $k$  for different values of the dispersion parameter  $C_S$ . The plots of Fig. 4(a) correspond to the CNLS equation (6c) with the nonlinear coefficient (8), while Figs. 4(b) and 4(c) are associated with the nonlinear coefficient (7c) for  $C_S < C_S^0$  and  $C_S > C_S^0$ , respectively. Figures 2(a) and 4(a) show that the region of modulational stability (MS) (i.e.,  $PQ < 0$ ) under the CNLS equation (6c) with the nonlinear coefficient (8) is enhanced when the dispersion parameter  $C_S$  increases. Figures 2(a) and 4(b) show that the region of modulational stability (i.e.,  $PQ < 0$ ) under the CNLS equation (6c) with the nonlinear coefficient (7c) shrinks when the dispersion parameter  $C_S < C_S^0$  increases. It can be seen from Figs. 2(a) and 4(c) that using the nonlinear coefficient (7c), the region of modulational stability (i.e.,  $PQ < 0$ ) shrinks for low frequencies and is enhanced for high frequencies when  $C_S > C_S^0$  increases. In other words, the size of the interval  $[f_{\min}, f_z]$  decreases (here  $f_z \downarrow$ ) while the size of the interval

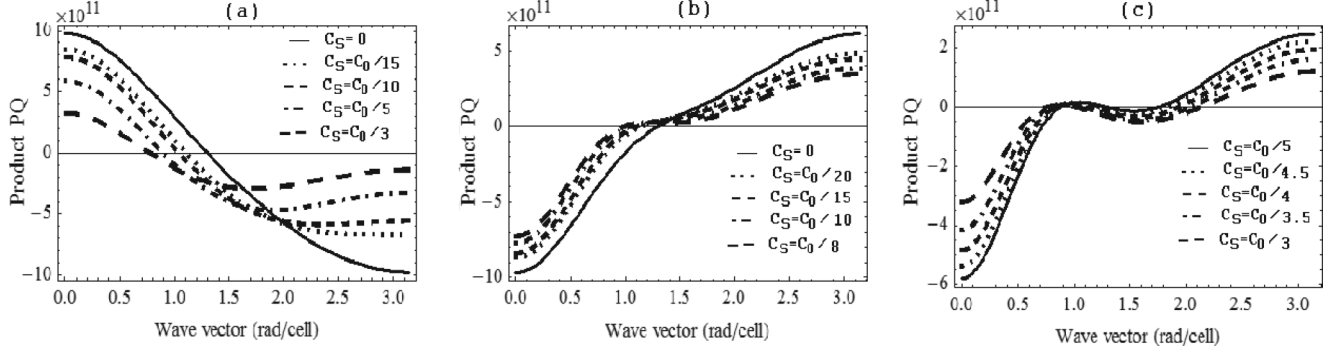


FIG. 4. Plots of  $PQ$  showing the regions of positive and negative  $PQ$  for different values of the dispersion parameter  $C_S$ . (a) Plot of product  $PQ$  with the nonlinear coefficient  $Q$  given by Eq. (8) for different  $C_S$ . (b) Plot of product  $PQ$  generated with the nonlinear coefficient (7c) for different parameters  $C_S < C_S^0 \approx C_0/5.8675457875$ . (c) Plot of product  $PQ$  generated with the nonlinear coefficient (7c) for different parameters  $C_S > C_S^0 \approx C_0/5.8675457875$ . These plots are generated with line parameters (3).

$]f_{q_1}, f_{q_2}[$  increases (here  $f_{q_1} \downarrow$  and  $f_{q_2} \uparrow$ ) when  $C_S > C_S^0$  increases.

### III. DYNAMICS OF BRIGHT AND DARK ONE-SOLITON WAVES IN LOSSLESS 1D NONLINEAR DISCRETE BI-INDUCTANCE TRANSMISSION LINES

In the present section, we use the classical nonlinear Schrödinger equation (6c) with the dispersion coefficient (7b) and nonlinear coefficient  $Q$  given by either Eq. (7c) or (8) to study the dynamics of bright and dark one-dimensional solitary waves in the electrical network shown in Fig. 1.

#### A. Analytical solutions of the classical nonlinear Schrödinger equation

We focus on solutions on the nonvanishing cw background

$$V_{01c}(\xi, \tau) = \begin{cases} A_{cb} \exp(i\phi_{cb}) & \text{for } PQ > 0 \\ -A_{cd} \sqrt{-Q/2P} \exp(i\phi_{cd}) & \text{for } PQ < 0, \end{cases}$$

with

$$\begin{aligned} \phi_{cb} &= k_{cb} \sqrt{\frac{Q}{2P}} \xi + \frac{Q}{2} (2A_{cb}^2 - k_{cb}^2) \tau, \\ \phi_{cd} &= k_{cd} \xi - \frac{A_{cd}^2 Q^2 + 2P^2 k_{cd}^2}{2P} \tau + \delta_0, \end{aligned}$$

where  $A_{cb}$ ,  $A_{cd}$ ,  $k_{cb}$ ,  $k_{cd}$ , and  $\delta_0$  are arbitrary real constants. After performing the Darboux transformation [27,28] for the CNLS equation (6c), we use the above nonvanishing cw background  $V_{01c}(\xi, \tau)$  to obtain the bright and dark soliton solutions

$$\begin{aligned} V_{01}(\xi, \tau) &= \left( A_{cb} + A_{sb} \frac{d_1 \cosh \theta + \cos \varphi}{\cosh \theta + d_1 \cos \varphi} + i A_{sb} \frac{d_2 \sinh \theta + d_3 \sin \varphi}{\cosh \theta + d_1 \cos \varphi} \right) \\ &\quad \times \exp(i\phi_{cb}), \end{aligned} \quad (9)$$

$$V_{10}(\xi, \tau) = -\sqrt{-\frac{Q}{2P}} (A_{cd} + i A_{sd} \tanh \zeta) \exp(i\Phi_{cd}), \quad (10)$$

respectively. In the solutions (9) and (10), the solution parameters are defined as

$$\begin{aligned} \theta &= M_R \sqrt{\frac{Q}{2P}} \xi - \frac{(k_{cb} + k_{sb})M_R - A_{sb}M_I}{2} Q\tau - \theta_0, \\ \varphi &= M_I \sqrt{\frac{Q}{2P}} \xi - \frac{(k_{cb} + k_{sb})M_I + A_{sb}M_R}{2} Q\tau - \varphi_0, \\ \zeta &= A_{sd} \frac{Q}{2P} \xi + \frac{A_{sd}(A_{cd}Q^2 - 4P^2k_{cd}^2)}{2P} \tau + \zeta_0, \\ \Phi_{cd} &= k_{cd}\xi - \frac{Q^2(A_{sd}^2 + A_{cd}^2) + 2k_{cd}^2P^2}{2P} \tau + \delta_0, \\ d_1 &= \frac{A_{cb}(M_R - A_{sb})}{D}, \quad d_2 = \frac{A_{cb}(k_{sb} - k_{cb} + M_I)}{D}, \\ d_3 &= \frac{D - 2A_{cb}^2}{D}, \\ D &= A_{cb}^2 + \frac{(M_R - A_{sb})^2 + (k_{sb} - k_{cb} + M_I)^2}{4}, \\ M &= \sqrt{(-A_{sb} + ik_{sb} - ik_{cb})^2 - 4A_{cb}^2} = M_R + iM_I, \end{aligned}$$

and  $A_{sb}$ ,  $A_{sb}$ ,  $\theta_0$ ,  $\varphi_0$ ,  $k_{sb}$ ,  $\zeta_0$ , and  $k_{sd}$  are arbitrary real constants. The bright soliton solution (9) and the dark soliton solution (10) have the following properties. They turn into the above cw background solution  $V_{01c}(\xi, \tau)$  when  $A_{sb} = 0$  and when  $A_{sd} = 0$ , respectively. On the other hand, in the absence of the cw background, i.e., when  $A_{cb} = 0$  and when  $A_{sd} = 0$ , they respectively turn into the bright soliton

$$\begin{aligned} V_{01}(\xi, \tau) &= \frac{A_{sb} \exp \{ i [k_{sb} \sqrt{Q/2P} \xi - (k_{sb}^2 - A_{sb}^2)(Q\tau/2) - \varphi_0] \}}{\cosh [A_{sb}(\sqrt{Q/2P} \xi - k_{sb} Q\tau - \xi_0)]} \end{aligned} \quad (11)$$

and the kink soliton solution

$$\begin{aligned} V_{10}(\xi, \tau) &= -i A_{sd} \sqrt{-\frac{Q}{2P}} \tanh \left( \frac{Q A_{sd}}{2P} \xi - \xi_0 \right) \\ &\quad \times \exp \left[ i \left( -\frac{A_{sd}^2 Q^2}{2P} \tau - \tau_0 \right) \right], \end{aligned} \quad (12)$$

where  $\xi_0$  and  $\tau_0$  are two arbitrary real constants. Therefore, the exact solutions (9) and (10) describe solitary waves embedded on a cw background.

Inserting the expressions (9) and (10) in Eqs. (6a) and (6b), we obtain the analytical expressions for  $V_{02}(\xi, \tau)$  and  $V_{12}(\xi, \tau)$ . Inserting the analytical expressions of  $V_{10}(\xi, \tau)$ ,  $V_{02}(\xi, \tau)$ , and  $V_{12}(\xi, \tau)$  in the general form (5) of the voltage  $V_n(t)$  and returning to the original coordinates  $n$  and  $t$  by means of Eq. (4) leads to the analytical expressions for the voltage  $V_n(t)$ . These analytical expressions for  $V_n(t)$  will be used to investigate the dynamics of matter-wave solitons in the network. Next, we separately discuss the dynamics of matter-wave solitons in the region of modulational instability (MI) [envelope solitons given by the analytical expression (9)] and in the region modulational stability [hole solitons defined by Eq. (10)].

### B. Dynamics of matter-wave solitons in the regions of MI ( $PQ > 0$ )

Using the zeros of the functions  $P = P(k)$  and  $Q = Q(k)$ , we have shown, for a given set of line parameters, the regions of the MI for the CNLS equation (6c) with the nonlinear coefficient (7c) or (8) in Fig. 3. In the regions of MI ( $PQ > 0$ ), the matter-wave solitons are envelope solitons propagating on the cw background and defined by the analytical expression (9). Without loss of generality, we restrict ourselves to the CNLS equation (6c) with the dispersion coefficient (7b). It follows from the above solution coefficients that

$$M|_{k_{sb}=k_{cb}} = \sqrt{A_{sb}^2 - 4A_{cb}^2}$$

$$= \begin{cases} i\sqrt{4A_{cb}^2 - A_{sb}^2} = iM_I & \text{for } 4A_{cb}^2 - A_{sb}^2 > 0 \\ 0 = 0M_R + 0R_I & \text{for } 4A_{cb}^2 - A_{sb}^2 = 0 \\ \sqrt{A_{sb}^2 - 4A_{cb}^2} = M_R & \text{for } 4A_{cb}^2 - A_{sb}^2 < 0, \end{cases}$$

with the case  $4A_{cb}^2 - A_{sb}^2 = 0$  leading to a constant solution. We focus on the following four special cases: (i)  $A_{cb} = 0$ , (ii)  $k_{sb} = k_{cb}$  and  $A_{sb}^2 - 4A_{cb}^2 < 0$ , (iii)  $k_{sb} = k_{cb}$  and  $A_{sb}^2 - 4A_{cb}^2 > 0$ , and (iv)  $A_{cb}A_{sb}(4A_{cb}^2 - A_{sb}^2)(k_{sb} - k_{cb}) \neq 0$ .

#### 1. Case $A_{cb} = 0$

In the case  $A_{cb} = 0$ , the solution (9) of the CNLS equation (6c) under the condition  $PQ > 0$  [i.e., solution (11)] can be written in the form

$$V_{10}(\xi, \tau) = \frac{A_{sb}}{\cosh[A_{sb}(\sqrt{Q/2P}\xi - k_{sb}Q\tau - \xi_0)]} \exp(i\Psi), \quad (13)$$

with

$$\Psi(\xi, \tau) = k_{sb}\sqrt{\frac{Q}{2P}}\xi - \frac{(k_{sb}^2 - A_{sb}^2)Q}{2}\tau - \varphi_0,$$

where  $\varphi_0$  and  $\xi_0$  are two arbitrary real constants. The expression (13) is just an envelope soliton solution of the CNLS equation (6c) under the condition  $PQ > 0$ . The solution (13) reveals that the envelope soliton is  $\eta(\tau) = \sqrt{2P/Q}(k_{sb}Q\tau + \xi_0)$  and the width of the envelope soliton is inversely proportional to  $\sqrt{Q/2P}$ . This means that we can use Eq. (13) to describe the compression (extension)

of envelope solitons in a given network when  $\sqrt{Q/2P}$  increases with the wave frequency  $f = \omega/2\pi$ . It is obvious that

$$\lim_{k \rightarrow k_z \text{ with } P(k)Q(k) > 0} \sqrt{\frac{Q}{2P}} \nearrow +\infty,$$

meaning that for a given set of network parameters, the width of the envelope soliton shrinks as the frequency

$$f(k) = \frac{\omega}{2\pi} \xrightarrow{PQ > 0} f_z = f(k_z).$$

Also, it is shown that the soliton center moves with the constant velocity  $d\eta/d\tau = k_{sb}Q\sqrt{2P/Q}$ . In what follows we take some examples to demonstrate the dynamics of envelope soliton in the network of Fig. 1.

As the first example we consider the line parameters (3) with  $C_S = C_0/5$ . For these line parameters, the regions of negativity of  $PQ$  (i.e., the regions of existence of envelope solitons) are (in MHz) the region of low frequencies  $f \in [1.998\,94, 2.112\,54[$  and the region of higher frequencies  $f \in [2.230\,66, 2.363\,1[$ . The function  $\sqrt{Q/2P}$  decreases for  $f \in [1.998\,94, 2.112\,54[$  and increases for  $f \in [2.230\,66, 2.363\,1[$ . With the present line parameters, we depict in Fig. 5 the time evolution of the voltage  $V_n(t)$  at cell  $n = 1$  for different wave frequencies. Figures 5(a)–5(c) show the waves propagating with low frequencies, while Figs. 5(d)–5(f) show waves propagating with high frequencies. It can be seen in Figs. 5(a)–5(c) that the width of the envelope solitons increases as the wave frequency increases. Figures 5(d)–5(f) show that the width of the envelope solitons decreases as the wave frequency increases. These two phenomena are justified by the fact that quantity  $\sqrt{Q/2P}$  (which describes either the compression or the extension of the solitons) is a decreasing function (an increasing function) of frequency  $f$  in the region of low frequencies (in the region of higher frequencies).

For our second example we consider three networks with the same line parameters (3) except the dispersion parameters  $C_S$  taken from the interval  $[90, 180]$  (we note that each value of the parameter  $C_S$  is associated with one network). We consider waves with propagation frequencies associated with wave vectors  $k = 1.016$  and  $2.4$  rad. With both of these wave vectors, the frequency  $f = \omega/2\pi$  decreases as a function of the dispersion parameter  $C_S$  in the interval  $[0, C_0/2]$  (see Fig. 2). Figure 6 shows the temporal evolution of the voltage  $V_n(t)$  of cell  $n = 1$  for three values of  $C_S = C_0/5$ ,  $C_0/4.5$ , and  $C_0/4$ . Figures 6(a)–6(c) and 6(d)–6(f) are obtained with lower frequencies and higher frequencies, respectively. Figures 6(a) and 6(d), 6(b) and 6(e), and 6(c) and 6(f) correspond to the same network, respectively. The plots of this figure show the extension of the envelope solitons when the propagating frequency decreases. Figures 6(a)–6(c) and 6(d)–6(f) also reveal that the width of the envelope soliton increases when the dispersion parameter  $C_S$  increases. Therefore, we can use the parameter  $C_S$  to control the soliton width in the MI regime.

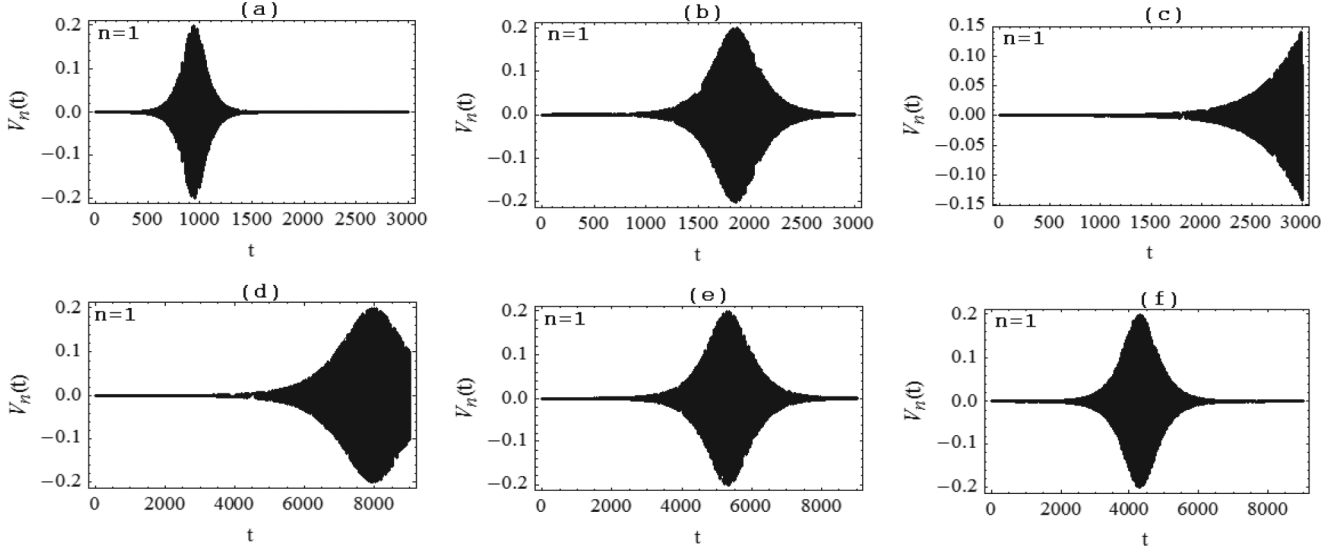


FIG. 5. Wave propagation in the region of low frequencies (top) and in the region of higher frequencies (bottom) showing the extension and the compression of envelope solitons, respectively. These plots are obtained with line parameters (3) with  $C_S = C_0/5$  and  $\varepsilon = 10^{-3}$ ,  $A_{sb} = 10$ ,  $k_{sb} = -0.6$ ,  $\xi_0 = -10$ , and  $\varphi_0 = 0$ . We used the frequencies (a)  $f = 2.018$  MHz, (b)  $f = 2.047$  MHz, (c)  $f = 2.077$  MHz, (d)  $f = 2.247$  MHz, (e)  $f = 2.265$  MHz, and (f)  $f = 2.281$  MHz.

### 2. Case $k_{sb} = k_{cb}$ and $A_{sb}^2 - 4A_{cb}^2 < 0$

In the present case, the solution (9) becomes

$$V_{01}(\xi, \tau) = \left( A_{cb} + A_{sb} \frac{-A_{sb} \cosh \theta + 2A_{cb} \cos \varphi + i\sqrt{4A_{cb}^2 - A_{sb}^2} \sinh \theta}{2A_{cb} \cosh \theta - A_{sb} \cos \varphi} \right) \exp \left[ i \left( k_{cb} \sqrt{\frac{Q}{2P}} \xi + \frac{Q}{2} (2A_{cb}^2 - k_{cb}^2) \tau \right) \right], \quad (14)$$

with  $\theta = (A_{sb} \sqrt{4A_{cb}^2 - A_{sb}^2} / 2) Q \tau - \theta_0$  and  $\varphi = \sqrt{4A_{cb}^2 - A_{sb}^2} (\sqrt{Q/2P} \xi - k_{cb} Q \tau) - \varphi_0$ , where  $\theta_0$  and  $\varphi_0$  are two arbitrary real constants. It follows from the expressions of  $\theta$  and  $\varphi$  and the transformation (4) that the solution (5) associated with the solution (14) is periodic with the period  $(2\pi/\varepsilon) \sqrt{2P/Q} (4A_{cb}^2 - A_{sb}^2)$  in the spatial coordinate  $n$  and aperiodic in the temporal coordinate  $t$  as soon as the wave vector of the cw background is chosen from the condition  $k_{cb} = \tilde{k} \sqrt{4A_{cb}^2 - A_{sb}^2}$ , where  $\tilde{k}$  is any integer. Any wave vector  $k_{cb} \neq \tilde{k} \sqrt{4A_{cb}^2 - A_{sb}^2}$  leads to an aperiodic solution in both temporal and spatial coordinates.

Figure 7 shows the evolution of the MI corresponding to the solution (14) with line parameter (3) for the dispersion parameter  $C_S = C_0/5$ . Figures 7(a)–7(c) and 7(d)–7(f) show the transmission of the wave through the network for frequencies  $f = 2.018$  and 2.256 MHz, respectively. Therefore, the envelope soliton of Figs. 7(a)–7(c) propagates with a frequency taken from the region  $[f_{\min}, f_z]$  of the MI, while the soliton wave of Figs. 7(g) and 7(h) is associated with frequency taken from the region  $[f_{q_2}, f_{\max}]$  of the MI. Figures 7(g) and 7(h) show solitons propagating with different frequencies taken from the same region of the MI. From this figure, it can be clearly seen that the cw background becomes unstable. Figure 7 shows that the choice of the propagating frequency in the region of the MI affects the soliton propagation in a given network. This figure also reveals that with a best choice of solution parameters, the soliton wave appears to be periodic

in the time coordinate and the period in the time coordinate increases with the wave frequency. This can be clearly seen in Figs. 7(c) and 7(f), as well as in Figs. 7(g) and 7(h). Moreover, as we can see from Figs. 7(g) and 7(h), the envelope soliton has different behavior when propagating at a frequency taken from the region of low frequencies and at a frequency taken from the region of high frequencies of the MI. We can conclude from Figs. 7(g) and 7(h) that the period of the propagating wave with respect to the time coordinate  $t$  is somehow connected to the frequency  $f$  of the envelope soliton: In the region of low frequencies of the MI, the period with respect to the time coordinate  $t$  increases with the wave frequency  $f$ , while in the region of high frequencies of the MI, the period with respect to the time coordinate decreases as the wave frequency increases.

### 3. Case $k_{sb} = k_{cb}$ and $A_{sb}^2 - 4A_{cb}^2 > 0$

In the case  $k_{sb} = k_{cb}$  and  $A_{sb}^2 - 4A_{cb}^2 > 0$ , we can compute the coefficients of the solution (9) and obtain the solution in the form

$$V_{01}(\xi, \tau) = \left( -A_{cb} + \frac{\sqrt{A_{sb}^2 - 4A_{cb}^2} (\sqrt{A_{sb}^2 - 4A_{cb}^2} \cos \varphi - i A_{sb} \sin \varphi)}{A_{sb} \cosh \theta - 2A_{cb} \cos \varphi} \right) \times \exp \left[ i \left( k_{cb} \sqrt{\frac{Q}{2P}} \xi + \frac{Q}{2} (2A_{cb}^2 - k_{cb}^2) \tau \right) \right], \quad (15)$$

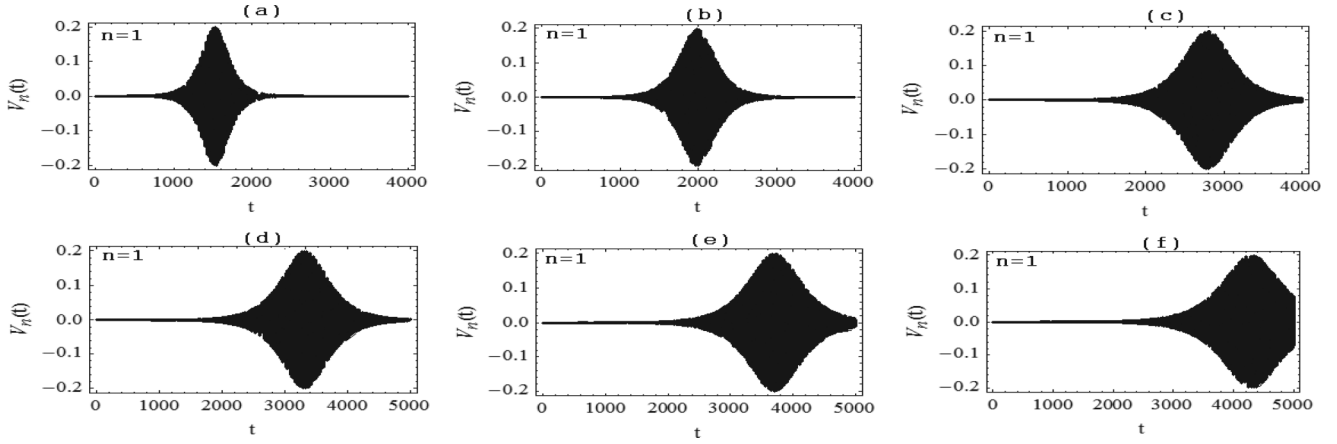


FIG. 6. Temporal evolution of the soliton waves propagating with frequencies taken from the region of (a)–(c) lower frequencies and (d)–(f) higher frequencies corresponding to different dispersion parameters  $C_S$  given in the text: (a)  $C_S = C_0/5 \iff f = 2.037$  MHz, (b)  $C_S = C_0/4.5 \iff f = 2.020$  MHz, (c)  $C_S = C_0/4 \iff f = 2.00$  MHz, (d)  $C_S = C_0/5 \iff f = 2.327$  MHz, (e)  $C_S = C_0/5 \iff f = 2.275$  MHz, and (f)  $C_S = C_0/4 \iff f = 2.215$  MHz. The solution parameters are the same as in Fig. 5.

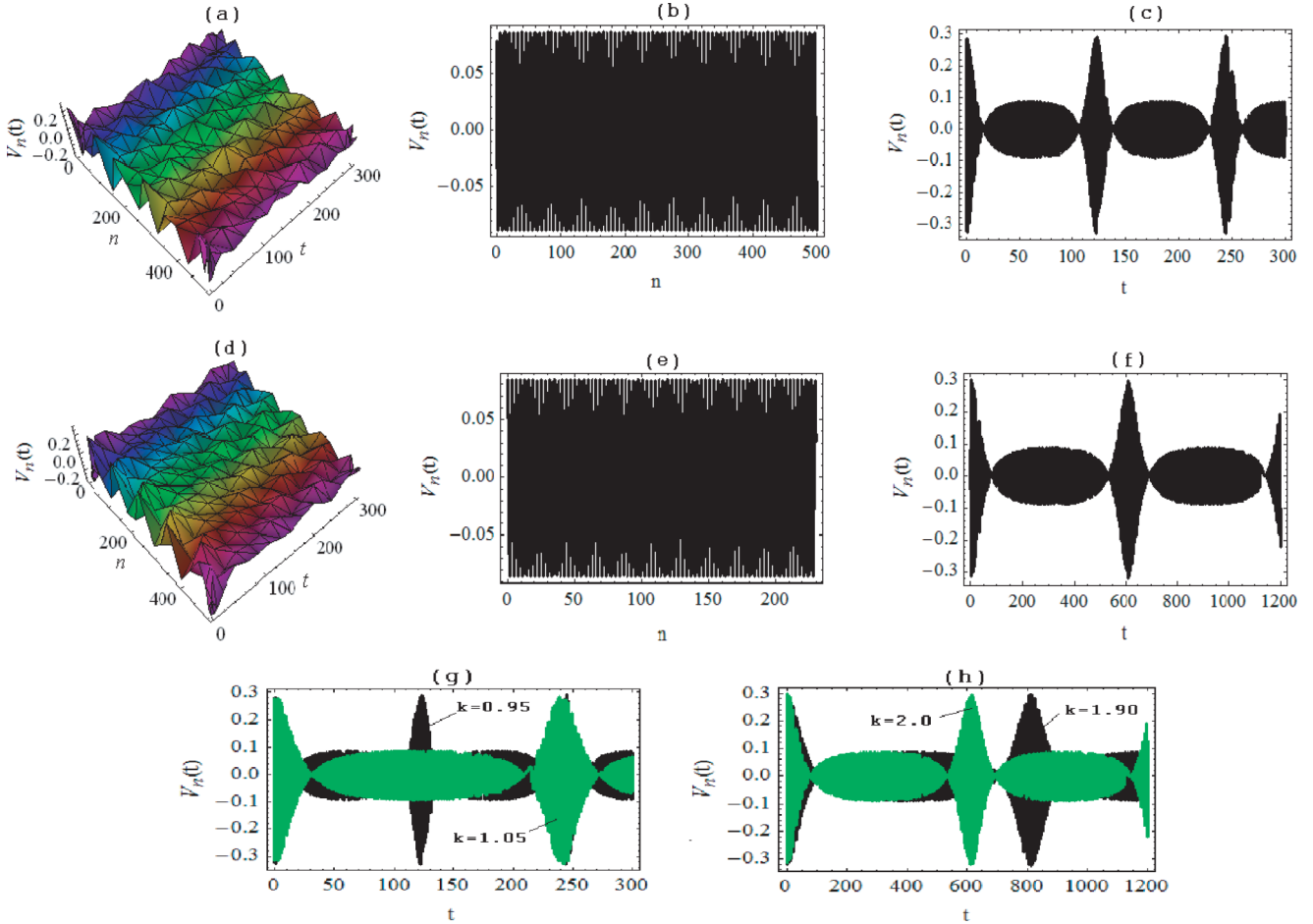


FIG. 7. (Color online) Evolution of modulational instability associated with Eq. (14) for line parameters (3) with the dispersion coefficient  $C_S = C_0/5$  and the frequency taken from the region of (a)–(c) lower frequencies  $f = 2.018$  MHz and (d)–(f) higher frequencies  $f = 2.273$  MHz. (a) and (d) Spatiotemporal evolution of the signal voltage, (b) and (e) spatial profile of the signal voltage at time  $t = 50$ , (c) and (f) temporal evolution of the signal voltage at cell  $n = 350$ , (g) time evolution of the signal voltage (at cell  $n = 350$ ) propagating with frequencies taken from the region  $[f_{\min}, f_z]$  of the modulational instability ( $f = 2.018$  MHz  $\iff k = 0.90$  and  $f = 2.047$  MHz  $\iff k = 1.05$ ), and (h) time evolution of the signal voltage (at cell  $n = 350$ ) propagating with frequencies taken from the region  $[f_{g_2}, f_{\max}]$  of the modulational instability ( $f = 2.256$  MHz  $\iff k = 1.90$  and  $f = 2.273$  MHz  $\iff k = 2.0$ ). Different curves are generated with the solution parameters  $\varepsilon = 10^{-3}$ ,  $A_{sb} = 10^{-4}$ ,  $A_{cb} = A_{sb}/1.8$ ,  $k_{cb} = k_{sb} = 2\sqrt{4A_{cb}^2 - A_{sb}^2}$ ,  $\varphi_0 = 0$ , and  $\theta_0 = -10^{-8}$ .

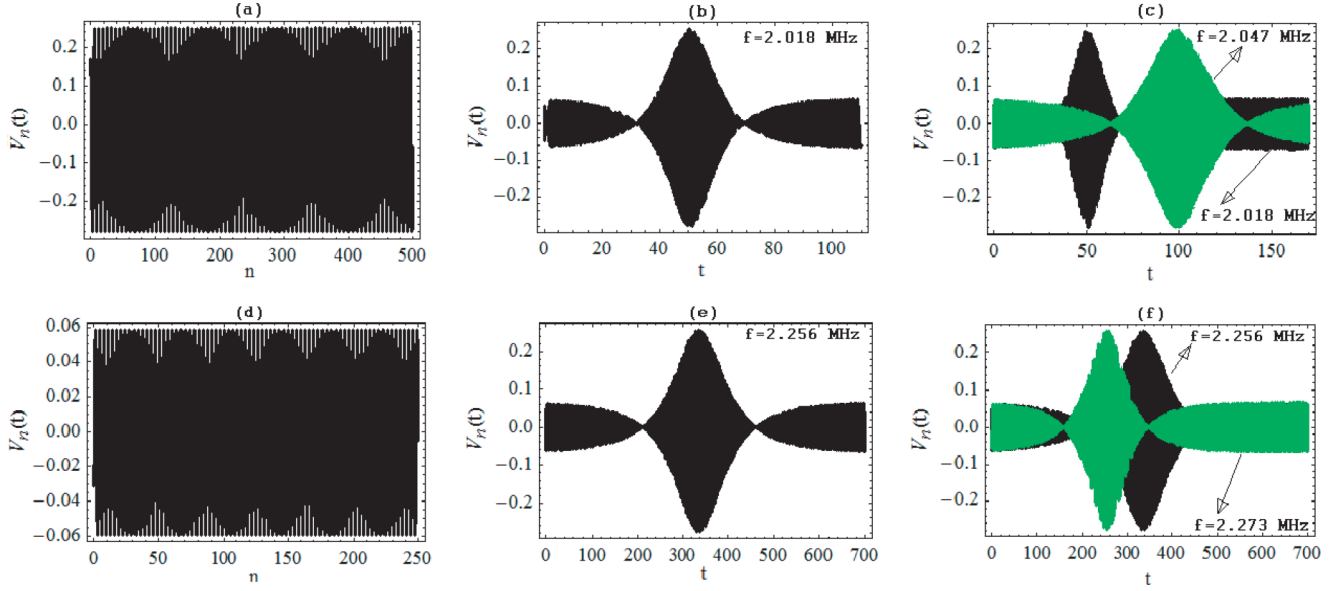


FIG. 8. (Color online) Evolution of envelope solitons on a cw background given by Eq. (15) for the same network as in Fig. 7 with the parameters  $\varepsilon = 10^{-3}$ ,  $A_{sb} = 10^{-4}$ ,  $A_{cb} = A_{sb}/3$ ,  $k_{cb} = 2\sqrt{A_{sb}^2 - 4A_{cb}^2}$ ,  $\varphi_0 = 0$ , and  $\theta_0 = -4$ . Spatial profile of bright solitons at time  $t = 50$  s propagating at frequencies (a)  $f = 2.018$  MHz and (d)  $f = 2.256$  MHz, time evolution of the envelope soliton in cell  $n = 350$  with frequencies (b)  $f = 2.018$  MHz and (e)  $f = 2.256$  MHz, and signal voltages of cell  $n = 350$  as a function of time  $t$  propagating with different frequencies taken from the region of (c) low frequencies of the modulational instability [ $f_{\min}, f_z$ ] and (f) high frequencies of the modulational instability [ $f_{g2}, f_{\max}$ ]. Different plots are generated with the same network parameters as in Fig. 7.

with  $\theta = \sqrt{A_{sb}^2 - 4A_{cb}^2}(\sqrt{Q/2P}\xi - k_{sb}Q\tau) - \theta_0$  and  $\varphi = -(QA_{sb}\sqrt{A_{sb}^2 - 4A_{cb}^2}/2)\tau - \varphi_0$ , where  $\theta_0$  and  $\varphi_0$  are two arbitrary real constants. It follows from the form of  $\theta$  and  $\varphi$  that the solution (15) is aperiodic in both spatial and temporal coordinates  $\xi$  and  $\tau$ . Returning to the original coordinates  $n$  and  $t$ , we can conclude that the movement of the envelope soliton is aperiodic in both  $n$  and  $t$  coordinates, as shown in Fig. 8. It can be seen in Figs. 8(c) and 8(f) that the

envelope solitons have different behavior when propagating at frequencies taken from the regions of low and high frequencies of the MI: For envelope solitons propagating at frequencies taken from the region of low frequencies of the MI, waves that propagate with smaller frequency reach their peak before those propagating with higher frequency. An inverse phenomenon is observed for envelope solitons propagating at frequencies taken from the region of high frequencies of the MI: A wave at large frequency reaches its peak before that at small frequency.

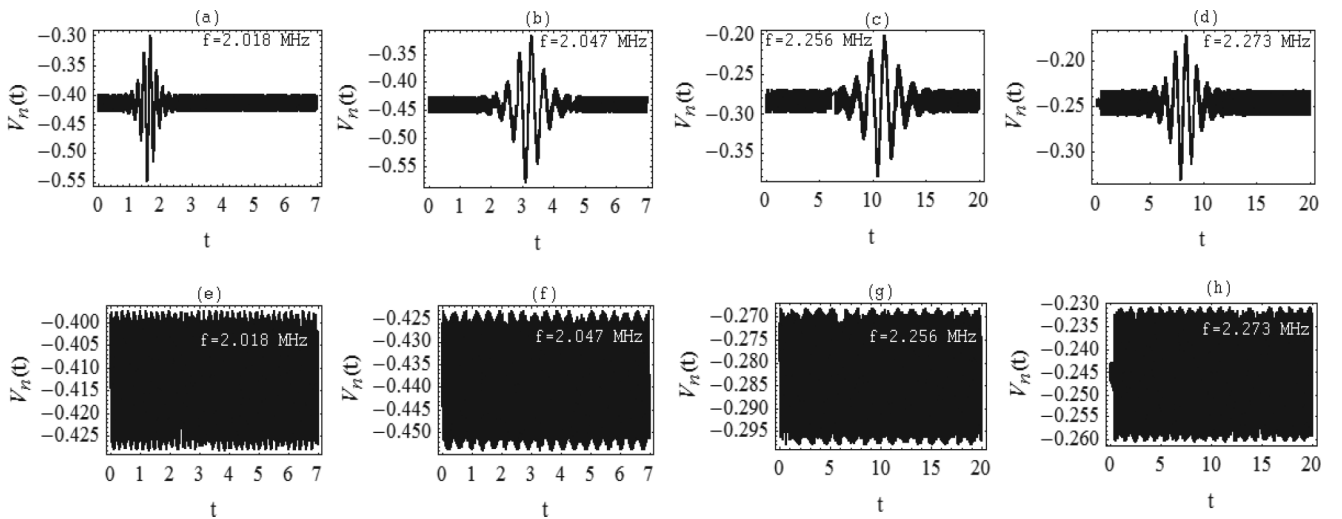


FIG. 9. Propagation of envelope solitons through the network for frequencies taken from different region of the MI. For the plots we use the line parameters (3) with  $C_S = C_0/5$  and  $\varepsilon = 10^{-3}$  and the solution parameters  $k_{cb} = 0.1$ ,  $k_{sb} = 0.2$ ,  $\varphi_0 = 0$ , and  $A_{cb} = \sqrt{k_{sb}(A_{sb}^2 + k_{cb}^2 - k_{sb}^2)}/2(k_{cb} + k_{sb})$ . The plots are obtained with (a)–(d)  $\theta_0 = -10$  and  $A_{sb} = 10^{-2}$  and (e)–(h)  $\theta_0 = -0.1$  and  $A_{sb} = 10^{-4}$ . Transmission of the envelope soliton through the 500th cell of the network for frequencies taken from the region of (a), (b), (e), and (f) low frequencies of the MI and (c), (d), (g), and (h) high frequencies of the MI.

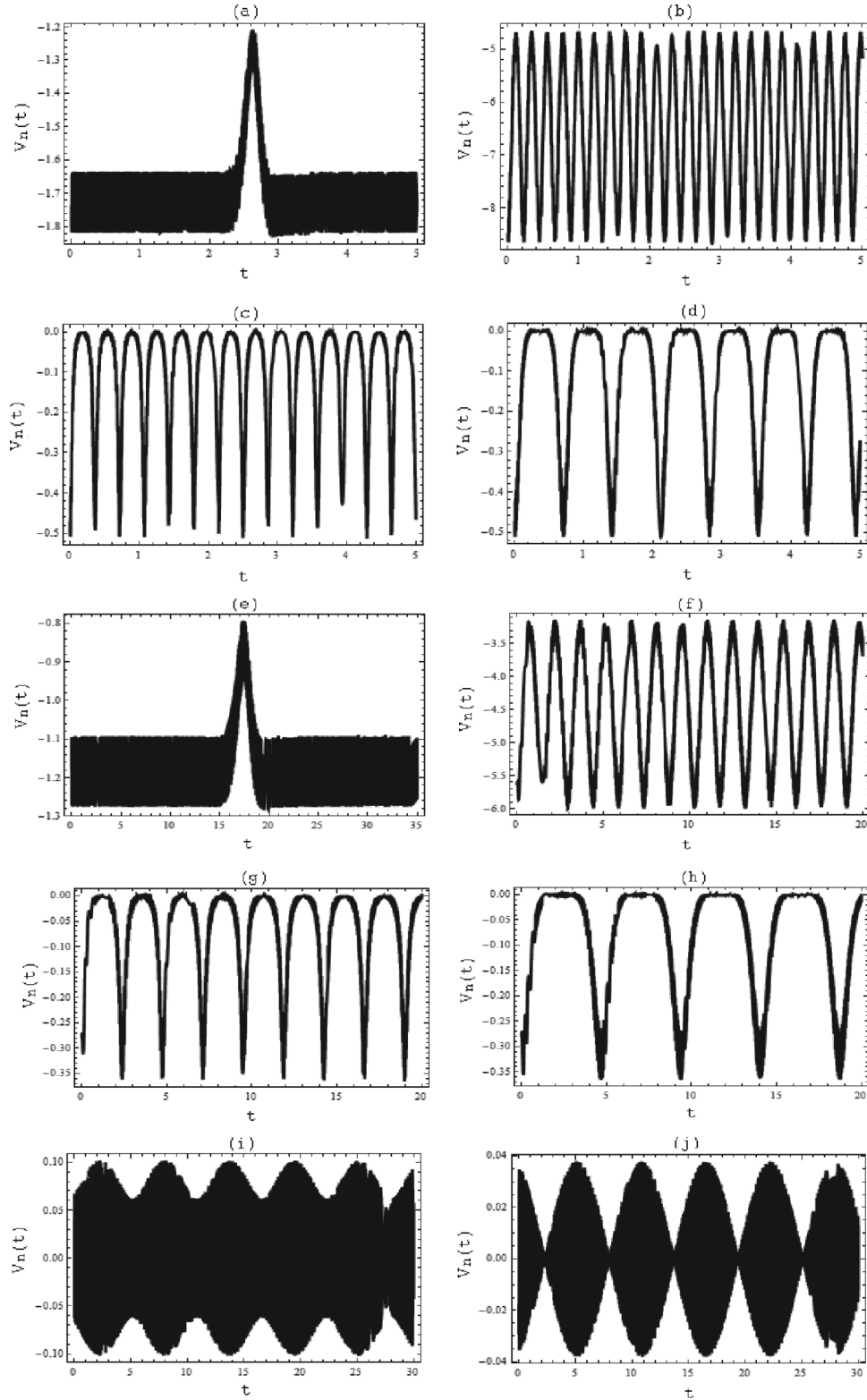


FIG. 10. Propagation of envelope solitons on the network parameters (3) for  $C_S = C_0/5$ . Signal voltage (in volts) at cell  $n = 350$  as a function of time  $t$  (in ms) for solution parameters (a) and (e)  $\theta_0 = -32.6$ ,  $A_{sb} = -10^{-2}$ ,  $A_{cb} = 0.041$ ,  $k_{sb} = 0.18$ , and  $k_{cb} = 0.19$ ; (b) and (f)  $\theta_0 = -3.12 \times 10^{-5}$ ,  $A_{sb} = 10^{-2}$ ,  $A_{cb} = 0.071$ ,  $k_{sb} = 0.19$ , and  $k_{cb} = 0.18$ ; (c) and (g)  $\theta_0 = -1.92 \times 10^{-5}$ ,  $A_{sb} = 10^{-2}$ ,  $A_{cb} = 0.9 \times 10^{-2}$ ,  $k_{sb} = 0.18$ , and  $k_{cb} = 0.19$ ; (d) and (h)  $\theta_0 = -0.98 \times 10^{-5}$ ,  $A_{sb} = 10^{-2}$ ,  $A_{cb} = 0.9 \times 10^{-2}$ ,  $k_{sb} = 0.19$ , and  $k_{cb} = 0.18$ ; (i)  $\theta_0 = 0.029$ ,  $A_{sb} = -10^{-2}$ ,  $A_{cb} = 0.041$ ,  $k_{sb} = 0.18$ , and  $k_{cb} = \pi/2$ ; and (j)  $\theta_0 = -0.033$ ,  $A_{sb} = 10^{-2}$ ,  $A_{cb} = 0.9 \times 10^{-2}$ ,  $k_{sb} = 0.18$ , and  $k_{cb} = \pi/2$ . Other parameters are given in the text.

#### 4. Case $A_{cb}A_{sb}(4A_{cb}^2 - A_{sb}^2)(k_{sb} - k_{cb}) \neq 0$

In the case  $A_{cb}A_{sb}(4A_{cb}^2 - A_{sb}^2)(k_{sb} - k_{cb}) \neq 0$ , we have the general expression (9) corresponding to envelope solitons propagating in the regions of the modulational instability of the network of Fig. 1. Here we limit ourselves to the investigation of the effects of solution parameters on the wave propagation. If we take the solution parameters  $A_{cb}$ ,  $k_{cb}$ ,  $A_{sb}$ , and  $k_{sb}$  from the conditions

$$A_{sb}^2 \neq 2k_{sb}(k_{cb} + k_{sb}), \quad A_{cb}^2 = \frac{k_{sb}(A_{sb}^2 + k_{cb}^2 - k_{sb}^2)}{2(k_{cb} + k_{sb})},$$

$$M_R^2 = \frac{A_{sb}^2(k_{cb} - k_{sb})}{k_{cb} + k_{sb}}, \quad M_I^2 = k_{cb}^2 - k_{sb}^2,$$

we obtain the solution (9) with  $\theta = M_R\sqrt{Q/2P}\xi - \theta_0$  and

$$\varphi = M_I\sqrt{\frac{Q}{2P}}\xi - \frac{Q[(k_{cb} + k_{sb})M_I + A_{sb}M_R]}{2}\tau - \varphi_0,$$

where  $\theta_0$  and  $\varphi_0$  are two arbitrary real constants. From the expressions for  $\theta$  and  $\varphi$ , we can see that the solution (9) with the above set of parameters is periodic with the period  $4\pi Q^{-1}/[(k_{cb} + k_{sb})M_I + A_{sb}M_R]$  in the temporal coordinate  $\tau$  and aperiodic in the spatial coordinate  $\xi = \varepsilon(n - v_g t)$ . This means that the oscillation of the wave along the time axis  $t$  is more pronounced, as shown in Fig. 9. Figure 9 shows an example of MI developed by the network. The plots of this figure are generated with the use of the solution (9) for

$A_{sb}A_{cb}(k_{sb} - k_{cb}) \neq 0$  and show the propagation of envelope solitons on a cw background. It appears that the mechanism of development of this instability is different from the well-known mechanism of MI described by Benjamin and Feir [26]. In Figs. 9(a), 9(b), 9(e), and 9(f), wave propagate at frequencies taken from the region  $]f_{\min}, f_z[$  of the modulational instability, while the envelope solitons whose time evolution is shown in Figs. 9(c), 9(d), 9(g), and 9(h) propagate at frequencies taken from region  $]f_{q_2}, f_{\max}[$  of the MI. Figure 9 shows how much the solution parameters may affect the transmission of the signal voltage in the network.

As the second example of soliton propagation in the present case, we show in Fig. 10 the temporal evolution of a bright soliton at cell  $n = 350$  of the network with parameters (3) for  $C_S = C_0/5$  and  $\varepsilon = 10^{-3}$ . Figures 10(a)–10(d) show the propagation of the envelope soliton at low frequency  $f = 2.018$  MHz ( $\in ]f_z, f_{q_1}[$ ), while Figs. 10(e)–10(h) show the propagation of the envelope soliton at high frequency  $f = 2.256$  MHz ( $\in ]f_{q_2}, f_{\max}[$ ); Figs. 10(i) and 10(j) show the envelope soliton propagating at a frequency  $f \rightarrow f_{\max}$ , that is, at a frequency associated with  $k = \pi/1.000\,001 \rightarrow \pi$ . This figure is obtained with many combination in the choice of the solution parameters  $A_{sb}$ ,  $A_{cb}$ ,  $k_{sb}$ ,  $k_{cb}$ , and  $\theta_0$ , with  $\varphi_0 = 0$ . Comparing other plots with those of Figs. 10(i) and 10(j) shows that when a wave packet travels along the lattice, it experiences velocity fluctuations that become more and more important with the increase of lattice effects [as we can see from Fig. 2(a), frequency  $f$  is an increasing

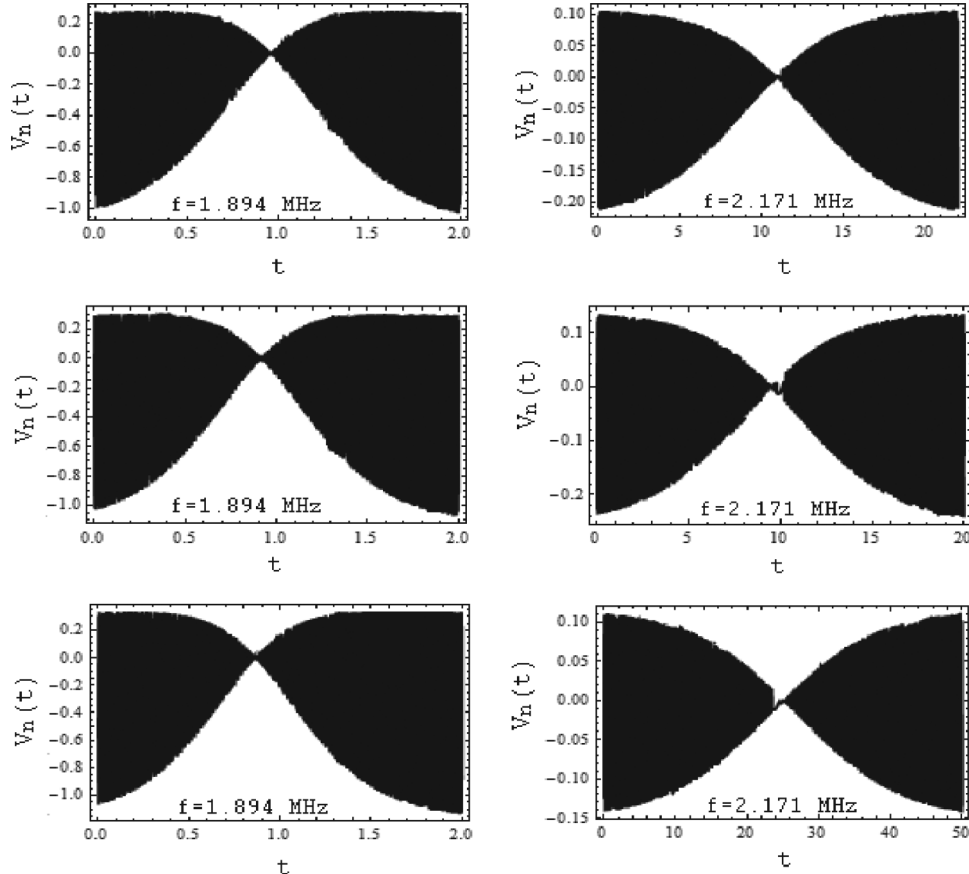


FIG. 11. Propagation of stable kink solitons through the network for the network parameters (3) with  $\varepsilon = 10^{-3}$  and with solution parameters  $k_{sd} = \pi/5$ ,  $A_{sd} = -10^{-2}$ ,  $\zeta_0 = 2$ , and  $\delta_0 = 0$  for  $C_S = C_0/5$  (top),  $C_S = C_0/4.5$  (middle), and  $C_S = C_0/4.1$  (bottom).

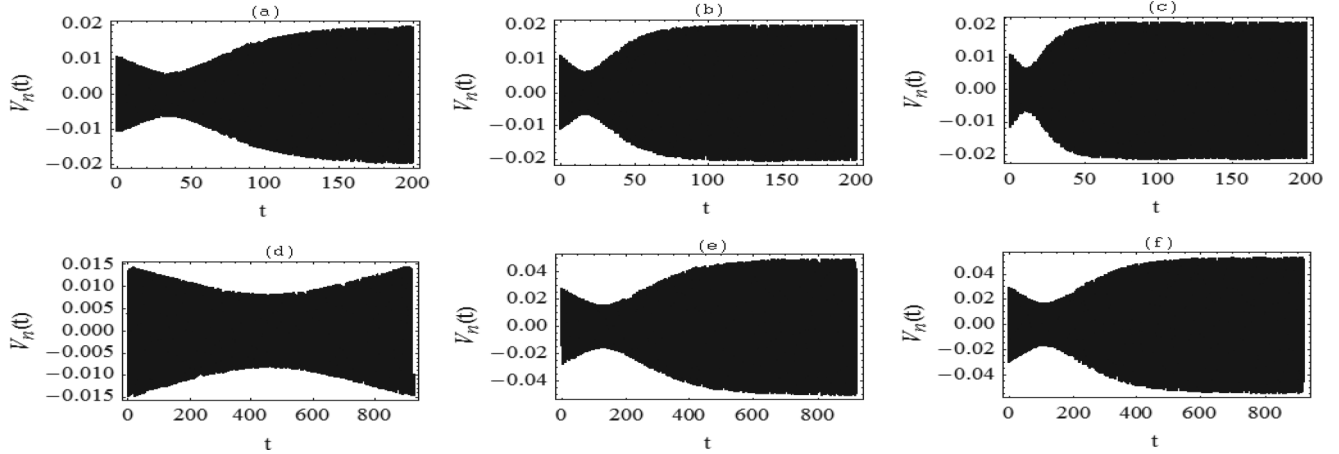


FIG. 12. Signal voltage (in volts) at cell  $n = 350$  as a function of time  $t$  (in ms). Temporal profile of dark solitons propagating on the network at different frequencies (in MHz) for line parameters (3) with  $C_S = C_0/5$ ,  $\varepsilon = 10^{-3}$ , and (a)  $f = 1.837$ , (b)  $f = 1.854$ , (c)  $f = 1.882$ , (d)  $f = 2.119$ , (e)  $f = 2.146$ , and (f)  $f = 2.171$ .

function of the lattice effect, i.e., increases with  $k$  so that any frequency from the region of low frequencies of the MI is less than any frequency from the region of high frequencies of the MI, which is less than frequency  $f(k \rightarrow \pi) = f_{\max}$ . Figure 10 shows that different combinations in the choice of the solution parameters lead to different scenarios of the propagation of signal voltage in the network (periodic pulses, aperiodic pulse, oscillatory waves, etc.).

### C. Dynamics of matter-wave solitons in the region of MS ( $PQ < 0$ )

With the help of the solution (10) we investigate in this section the dynamics of matter-wave solitons propagating in the network at frequencies taken from the regions of the modulational stability. As we have indicated above, the analytical solution (10) describes the propagation of dark (hole) solitons on the nonvanishing cw background  $V_{0lc}(\xi, \tau)$ . The analytical expression (10) shows that the soliton amplitude is proportional to  $\sqrt{-Q/2P}$ .

First, as it has been said above, in the absence of the cw background, i.e., when  $A_{cd} = 0$ , the solution (10) is associated with the propagation of a kink soliton through the network as it is shown in Fig. 11. Figure 11, obtained with the use of the CNLS equation (6c) with the nonlinear coefficient (7c), shows the temporal profile of stable kink solitary waves on the 350th cell at low frequencies (left column) and at high frequencies (right column). The top, middle, and bottom plots correspond to the network with the dispersion parameter  $C_S = C_0/5$ ,  $C_0/4.5$ , and  $C_0/4.1$ , respectively. The left and right panels of Fig. 11 show that independently of the value of the dispersion parameter  $C_S$ , the velocity of the soliton center decreases as the wave frequency increases.

Second, in the presence of the cw background (i.e.,  $A_{cb} \neq 0$ ), the solution (10) leads to propagation in the network of dark solitons embedded on a cw background. Thus, by employing the expression (10), we can obtain the dark soliton solution of Eq. (1), which propagates on a cw background. Figure 12 shows an example of the propagation of dark soliton on the network. Figures 12(a)–12(c) show dark solitons propagating at different frequencies taken

from the region  $[f_{\min}, f_z[$  of low frequencies of the MS, while Figs. 12(d)–12(f) show dark solitons propagating at different frequencies taken from the region  $]f_{q_1}, f_{q_2}[$  of high frequencies of the MS. To generate this figure, we have used the solution parameters  $k_{cd} = 0.1$ ,  $A_{cd} = -10^{-4}$ ,  $k_{sd} = 0.35$ ,  $A_{sd} = 3 \times 10^{-4}$ ,  $\delta_0 = 0$ , and  $\zeta_0 = -0.532$ .

## IV. CONCLUSION

In this work, we have investigated the dynamics of matter-wave solitons in lossless 1D nonlinear discrete bi-inductance electrical transmission lines. With the help of the reductive perturbation method in the semidiscrete limit, we have modeled the dynamics of modulated waves on the network by a classical nonlinear Schrödinger equations. Based on these CNLS equations, our analytical study predicts either two or four frequency regions with different behavior concerning the modulational instability of a plane wave. Performing the Darboux transformation for the derived CNLS equations, we have derived exact bright and dark one-dimensional solitons embedded in a cw background. With the help of these analytical solutions, we have investigated the transmission of soliton signals on the network. We found that the network under consideration may support the propagation of bright, dark, and kink soliton. We found that when a wave packet travels along the lattice, it experiences velocity fluctuations that become more and more important with the increase of lattice effects, that is, for  $k \rightarrow \pi$ . The analytical solutions imply that control of the dispersion parameter  $C_S$  allows us to manipulate the motion of bright, dark, and kink solitary waves in the network. The methodology presented here is powerful for systematically investigating the dynamics of matter-wave solitons in 1D nonlinear transmission lines. Our next challenge is to use the presented classical nonlinear Schrödinger equations to investigate the effects of the linear capacitance  $C_S$  on soliton-soliton interaction in the Noguchi network of Fig. 1.

## ACKNOWLEDGMENT

The authors would like to thank Prof. W. M. Liu of the IOP-CAS for his invaluable suggestions.

- [1] A. C. Scott, *Nonlinear Science: Emergence and Dynamics of Coherent Structures* (Oxford University Press, New York, 1999).
- [2] A. Hasegawa, *Optical Solitons in Fibers*, 2nd ed. (Springer, Berlin, 1989).
- [3] M. Remoissenet, *Waves Called Solitons*, 3rd ed. (Springer, Berlin, 1999).
- [4] N. J. Zabusky and M. D. Kruskal, *Phys. Rev. Lett.* **15**, 240 (1965).
- [5] K. Lonngren, in *Solitons in Action*, edited by K. Lonngren and A. Scott (Academic, New York, 1978).
- [6] T. Taniuti and N. Yajima, *J. Math. Phys.* **10**, 1369 (1969).
- [7] E. Kengne and R. Vaillancourt, *Can. J. Phys.* **87**, 1191 (2009).
- [8] E. Kengne, *J. Math. Phys.* **48**, 013508 (2007).
- [9] E. Kengne, V. Bozic, M. Viana, and R. Vaillancourt, *Phys. Rev. E* **78**, 026603 (2008).
- [10] T. Kakutani and N. Yamasaki, *J. Phys. Soc. Jpn.* **45**, 674 (1978).
- [11] A. C. Newell and J. V. Moloney, *Nonlinear Optics* (Addison-Wesley, Reading, 1991).
- [12] R. Hirota and K. Suzuki, *Proc. IEEE* **61**, 1483 (1973).
- [13] A. C. Scott, *Active and Nonlinear Wave Propagation in Electronics* (Wiley-Interscience, New York, 1970).
- [14] R. Marquié, J. M. Bilbault, and M. Remoissenet, *Physica D* **87**, 371 (1995).
- [15] E. Kengne and A. Lakhssassi, *Eur. Phys. J. B* **87**, 237 (2014).
- [16] E. Afshari and A. Hajimiri, *IEEE J. Solid-State Circ.* **40**, 744 (2005).
- [17] E. Kengne and W. M. Liu, *Phys. Rev. E* **73**, 026603 (2006).
- [18] F. B. Pelap and M. M. Faye, *J. Math. Phys.* **46**, 033502 (2005).
- [19] R. Hirota and K. Suzuki, *J. Phys. Soc. Jpn.* **28**, 1366 (1970).
- [20] A. Noguchi, *Electron. Commun. Jpn.* **57**, 9 (1974).
- [21] Y. H. Ichikawa, T. Mitsuhashi, and K. Konno, *J. Phys. Soc. Jpn.* **41**, 1382 (1976).
- [22] T. Yoshinaga and T. Kakutani, *J. Phys. Soc. Jpn.* **53**, 85 (1984).
- [23] M. Marklund and P. K. Shukla, *Phys. Rev. E* **73**, 057601 (2006).
- [24] E. Kengne, *J. Nonlin. Oscillations* **6**, 339 (2003).
- [25] P. Marquié, J. M. Bilbault, and M. Remoissenet, *Phys. Rev. E* **49**, 828 (1994).
- [26] T. B. Benjamin and J. E. Feir, *J. Fluid Mech.* **27**, 417 (1967).
- [27] Z. Xu, L. Li, Z. Li, and G. Zhou, *Phys. Rev. E* **67**, 026603 (2003).
- [28] B. Li, X.-F. Zhang, Y.-Q. Li, Y. Chen, and W. M. Liu, *Phys. Rev. A* **78**, 023608 (2008).